MAGNETOHYDRODYNAMICS Vol. 56 (2020), No. 2-3, pp. 103–111
DOI: 10.22364/mhd.56.2-3.1

MHD TAYLOR-COUETTE FLOW WITH INSULATING WALLS AT PERIODIC CONDITION AND LOW MAGNETIC REYNOLDS NUMBER

X.Y. Leng[1], *Yu.B. Kolesnikov*[2], *D. Krasnov*[2], *B.W. Li*[3]

[1] *Shanghai Key Laboratory of Special Artificial Microstructure Materials and Technology and School of Physics Science and Engineering, Tongji University, Shanghai 200092, China*
[2] *Institute of Thermodynamics and Fluid Mechanics, Ilmenau University of Technology, Ilmenau, Germany*
[3] *Institute of Thermal Engineering, School of Energy and Power Engineering, Dalian University of Technology, Dalian, China*
e-Mail: yuri.kolesnikov@tu-ilmenau.de

This work studies turbulent behavior in Taylor-Couette flow of an electrically conducting fluid between two co-axial and infinitely long insulating cylinders in the presence of an axial magnetic field at a low magnetic Reynolds number. The inner cylinder rotates and the outer one is kept stationary. Direct numerical simulation was conducted to study the problem with Reynolds numbers of 4000 and 8000 with different Hartmann numbers. The results show a continuous suppression of turbulence in the flow under the applied magnetic field. The mean flow profile is not directly affected by the magnetic field, but its transformation depends on the decrease of turbulent fluctuations and wall normal momentum transport. With increasing Hartmann number, the observed decrease of Taylor vortex flow is accompanied by the elongated axial wavelengths, confirming the theoretical prediction of linear stability theory. A comparison of the considered case of insulating cylinders with a previous study with conducting cylinders also indicates a difference between these two cases and highlights a significant impact of the electric boundary conditions on turbulence.

Introduction. The motion of an incompressible viscous fluid between concentric rotating cylinders, called Taylor-Couette flow, is a classical problem in hydrodynamics [1–4]. The simple configuration, but complex inherent phenomena, attract vast attention to nonlinear dynamics, stability analysis, bifurcation, and turbulence, with abundant consequences [3, 4]. In the theoretical calculations of Chandrasekhar [2], the stabilizing effect of the axial magnetic field on the first instability of Taylor-Couette flow is predicted. Recently, in our numerical works [5, 6], turbulence enhancement followed by laminarization has been explored for the case when the cylinders are electrically conducting and of equal potential. In a weak magnetic field, the induced radial electrical currents and the resulting Lorentz force modify the flow profile, creating strong shear near the inner cylinder which enhances the production of turbulent energy. In a strong magnetic field, turbulence dissipates and the flow transits to a laminar regime with the formation of negative velocity near the outer cylinder. Usually, in most experimental conditions, the side-wall cylinders are more likely electrically insulating as Plexiglass walls. The insulating walls would prevent the generation of radial (wall-normal) currents at the walls and hence of corresponding azimuthal Lorentz forces. Therefore, this setup differs from our previousely considered cases with conducting walls in a way that the magnetic field there does not modify the mean flow directly [5, 6].

In electrically conducting fluids, such as liquid metals used in laboratory and industry, the magnetic Reynolds number is usually very small, leading to other properties of the flow in contrast to the case of high magnetic Reynolds number [7]. For instance, magnetorotational instability (MRI) is considered as a powerful source to enhance the

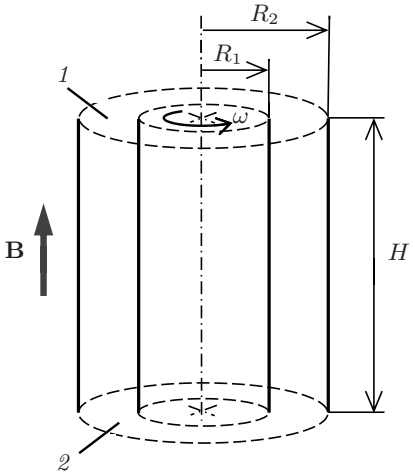

Fig. 1. Geometry of Taylor-Couette flow exposed to an axial magnetic field. Here R_1, R_2, and H stand, respectively, for the radii of inner and outer cylinders and for the height of the annulus. *1* and *2* denote top and bottom boundaries which are either periodic or Hartmann walls.

outward angular momentum transport in accretion disks, whereas weak magnetic fields can destabilize the motion and render the development of turbulent flow [8]. Nevertheless, in the limits of small magnetic Reynolds numbers, the applied field generally results in a stabilizing effect and exhibits a vortex motion [5, 6, 9, 10]. In the present work, we perform the study by direct numerical simulation (DNS) in the same geometry using a Dongs physical model [11] exposed to an axially applied magnetic field.

1. Presentation of the problem.

1.1. Equations and numerical methods. A three-dimensional (3D) flow of an incompressible viscous electrically conducting fluid considered here is contained in an annular channel between two concentric cylinders of radii R_1, R_2, and height H, as illustrated in Fig. 1. The fluid properties include the constant kinematic viscosity ν, the electrical conductivity σ, and the density ρ. It is assumed that the axes of the cylinders are aligned with the z-axis of the cylindrical coordinate system, and the inner cylinder rotates in counter-clockwise way, driving the liquid into rotation. The flow is subjected to an axial uniform magnetic field $\mathbf{B} = B \cdot \mathbf{e}_z$, where $\mathbf{e}_z$ is the unit vector in the axial direction. The dimensional variables, length, time, velocity, pressure, electric current density and magnetic field induction are normalized by the scales d, ω^{-1}, $\omega R_1 d$, $\rho(\omega R_1)^2$, $\sigma\omega R_1 B$, and B, respectively, where $d = R_2 - R_1$ and ω is the angular velocity of the inner cylinder. Thereafter the flow could be characterized by the following non-dimensional parameters: the Reynolds number $\mathrm{Re} = \omega R_1 d\nu^{-1}$, the Hartmann number $\mathrm{Ha} = Bd\sigma^{1/2}(\rho\nu^{-1/2})$, or alternatively, the Stuart number $\mathrm{N} = \mathrm{Ha}^2/\mathrm{Re}$ describing the ratio of Lorentz force to inertia force.

Similar to the previous studies, the computational domain was chosen from *1* to *2* in the radial direction, and from $-\pi$ to π in the periodic axial direction [5, 6, 11]. The corresponding radii ratio $\eta = R_1/R_2$ and the aspect ratio $\Gamma = H/d$ are 0.5 and 2π, respectively. In industrial and laboratory settings, liquid metals usually have a very

small magnetic Reynolds number, therefore, the quasi-static approximation is applied here [12]. Then, the dimensionless governing equations can be written as

$$\nabla \cdot \mathbf{u} = 0, \tag{1}$$

$$\frac{\partial \mathbf{u}}{\partial t} + (\mathbf{u} \cdot \nabla)\mathbf{u} = -\nabla p + \frac{1}{\mathrm{Re}}\nabla^2 \mathbf{u} + \frac{\mathrm{Ha}^2}{\mathrm{Re}}[\mathbf{j} \times \mathbf{e}], \tag{2}$$

$$\mathbf{j} = -\nabla \phi + [\mathbf{u} \times \mathbf{e}], \tag{3}$$

$$\nabla^2 \phi = \nabla \cdot [\mathbf{u} \times \mathbf{e}], \tag{4}$$

where t, p, and ϕ are, correspondingly, the time, the pressure and the electrical potential. Here $\mathbf{u}(u_r, u_\theta, u_z)$, $\mathbf{j}(j_r, j_\theta, j_z)$, and $\mathbf{e}(0, 0, 1)$ are the components of velocity, electrical current density, and the magnetic field unit vector in the radial, azimuthal and axial directions for cylindrical coordinates (r, θ, z), respectively. At the walls, no-slip boundary conditions for velocities are applied,

$$u_r = u_z = 0, \quad u_\theta = 1 \text{ at } r = 1 \text{ (inner cylinder)},$$

$$\mathbf{u} = 0 \text{ at } r = 2 \text{ (outer cylinder)};$$

and the perfectly insulating walls for electrical potential are

$$\partial\phi/\partial r = 1 \text{ and } 0, \text{ at } r = 1 \text{ and } 2,$$

assuming the condition of zero current density in the wall normal direction.

The system of equations (1)–(4) is solved numerically using the finite difference scheme [13]. The scheme is of the second order of approximation based on spatial discretization which is nearly fully conservative with regard to mass, momentum, kinetic energy, and electric charge conservation. The explicit Adams-Bashforth/Backward-Differentiation scheme of the second order is employed for time discretization. At every time step, two Poisson equations – the projection method equation for pressure and the equation for potential (4) – are solved using FFT in the azimuthal direction and the cyclic reduction direct solver [14]. Towards the walls, a clustered grid is implemented using a hyperbolic tangent coordinate transformation.

The numerical method and resolution tests have been verified in our earlier studies [5, 6]. In the present study, the grid arrangement is chosen as 321, 321 and 161 points in the azimuthal, axial and radial direction, correspondingly.

2. Main results.

2.1. Mean velocity profiles. In Figs. 2*a*,*b*, the profiles of mean azimuthal velocities are averaged in the axial and in the azimuthal direction, and in time. Hereafter, the symbol $\langle\rangle$ represents the results obtained through averaging transient 3D flow fields over the axial, azimuthal directions and time. At $\mathrm{Re} = 4000$ and 8000, without the magnetic field, the profiles represent a typical turbulent Taylor-Couette flow with two strong shear layers and flat cores. For the large Reynolds number in Fig. 2*b*, the thinner boundary layers correspond to stronger turbulence and, thus, steeper shear layers.

After imposing the axial magnetic field and due to its suppression effect, the turbulent fluctuations were damped, so the radial turbulent momentum transport got weaker, as illustrated in Figs. 3*a*,*b*. The turbulent boundary layers lose their turbulent features with the decreased mean shear rates. In the core flow, the flatten profiles enlarge and

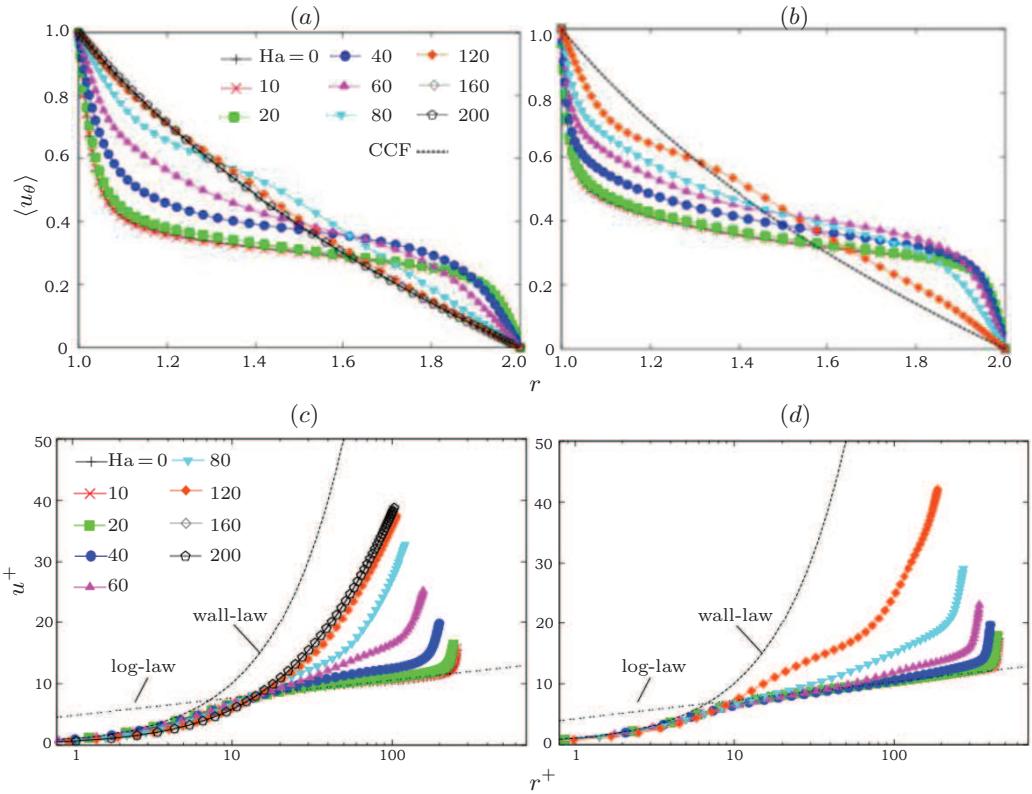

Fig. 2. Mean azimuthal velocity profiles $\langle u_\theta \rangle$ vs. Hartmann numbers: (*a*) $\mathrm{Re} = 4000$ and (*b*) $\mathrm{Re} = 8000$. Mean velocity profiles u^+ in wall units: (*c*) $\mathrm{Re} = 4000$ and (*d*) $\mathrm{Re} = 8000$. Mean velocity profiles u is normalized by the wall friction velocity $u^+ = (1 - \langle u_\theta \rangle)/u_\tau$ vs. wall units r^+, where r^+ is transformed by $r^+ = 2(r-1)\mathrm{Re}_\tau$. The wall friction velocity u_τ is defined as $u\tau^2 = \mathrm{Re}^{-1} r(\partial \langle u_\theta \rangle \partial r)$, and the friction Reynolds number as $\mathrm{Re}_\tau = 0.5 u_\tau \mathrm{Re}$.

approach the linear distribution of a circular Couette flow (CCF), since the momentum transported from the boundaries diminishes with the growth of Ha. In the lower Re cases, at a certain large value of Ha, the profiles coincide with those of CCF, indicating a relaminarization of the flow. Comparing with the previous results on conducting cylinders [6], the difference between the two kinds of electric boundary conditions becomes well apparent. For insulating cylinders, the radial currents at the walls are prevented, which limits the interaction between the mean radial current and the magnetic field. The observed suppression behavior is consistent with a straight MHD channel flow under a spanwise magnetic field [15]. For conducting cylinders [6], the mean profiles change dramatically with the turbulent enhancement process, yielding a region of negative velocity due to the negative azimuthal Lorentz force.

The effect of the magnetic field is further illustrated in Figs. 2*c*,*d* which show the mean profiles of the azimuthal velocity in wall units $u^+ = (1 - \langle u_\theta \rangle)/u_\tau$, where u_τ is the wall friction velocity $u\tau^2 = \mathrm{Re}^{-1} r(\partial \langle u_\theta \rangle \partial r)$, and the wall coordinate r^+ transformed as $r^+ = 2(r-1)\mathrm{Re}_\tau$. For both values of Re at $\mathrm{Ha} = 0$, the profiles demonstrate an almost perfect match to the classical logarithmic law behavior (shown by the log-law lines).

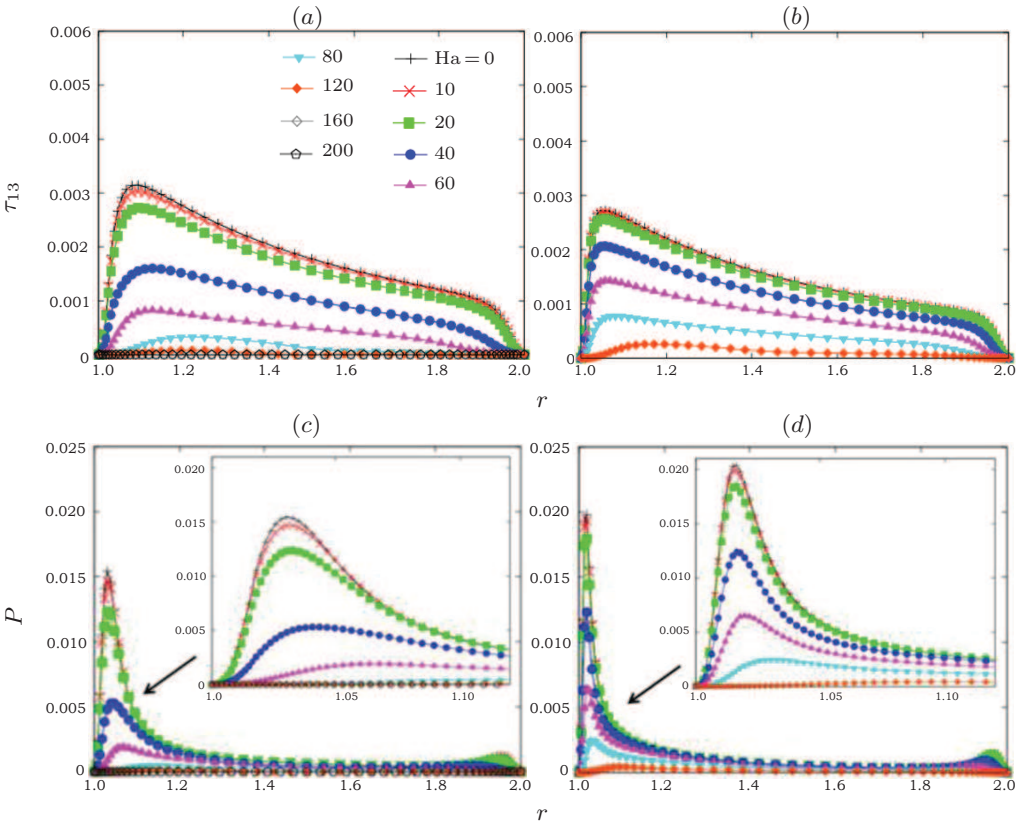

Fig. 3. Profiles of the Reynolds shear stress component $\tau_{13} = \langle u'_r u'_\theta \rangle$) corresponding to the wall-normal turbulent transport of streamwise velocity. (*a*) Re = 4000 and (*b*) Re = 8000. Distributions of the turbulent energy production $P = -\langle u'_r u'_\theta \rangle) r \partial \langle u_\theta / r \rangle \partial r$: (*c*) Re = 4000, and (*d*) Re = 8000.

Applying the magnetic field begins to suppress the turbulent fluctuations and, with increasing Ha, the curves deviate from the universal logarithmic law and exhibit a trend towards the laminar wall-law. It is explained by the balance between turbulent and laminar stresses. The growth of Ha gradually leads to damping of the turbulent stresses and the laminar counterpart begins to dominate not only near the wall, but also in the bulk. Thus, one can see a pronounced deviation from the log-law at high Ha which ceases at Ha = 80 for Re = 4000 and at Ha = 120 for Re = 8000. In the viscous sub-layer, the usual linear wall-law is sustained for all cases. The observed behavior is generally quite similar to that in our earlier study with conducting walls [6] and to that of a straight channel flow under a spanwise field [15].

2.2. Turbulent characteristics. Turbulent fluctuations can enhance the wall normal momentum transports. Due to the stronger shear driven, the wall normal Reynolds shear stresses have their peak values near the inner wall and are much larger than those near the outer walls, as shown in Figs. 3*a*,*b*. With increasing Ha, the smooth reduction processes are observed, and the complete suppression is also revealed at Re = 4000. The axial magnetic field damps the turbulent fluctuations via Joule dissipation directly. Unlike the scenario with conducting walls [6], because of the increasing mean shear rates

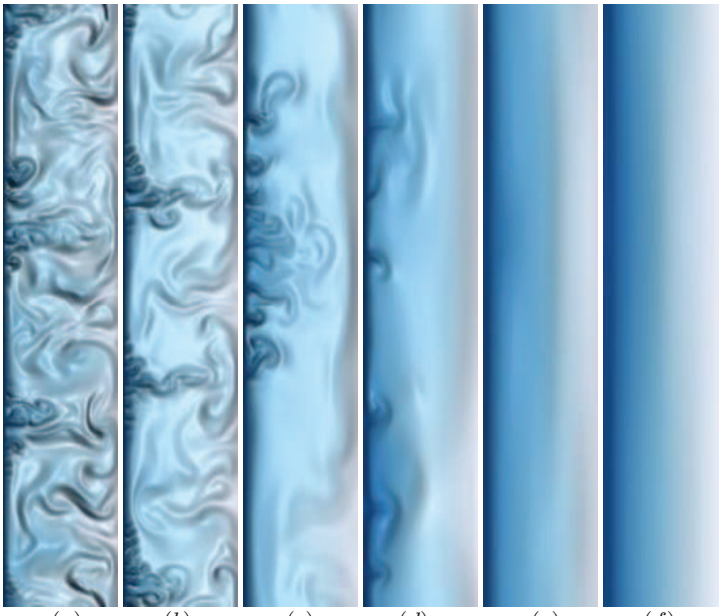

(*a*) (*b*) (*c*) (*d*) (*e*) (*f*)

Fig. 4. Instantaneous 2D contours of azimuthal velocity in meridional plane at Re = 4000 with varying Hartmann numbers. (*a*) Ha = 0, N = 0, (*b*) Ha = 20, N = 0.1, (*c*) Ha = 40, N = 0.4, (*d*) Ha = 60, N = 0.9, (e) Ha = 80, N = 1.6, and (*f*) Ha = 120, N = 3.6.

(transformation of mean profiles) resulting from the passing radial current, the turbulent fluctuations can exhibit an initial enhancing stage before the following suppression process.

The distributions of turbulent energy production illustrated in Figs. 3*c*,*d* show that the largest values of the turbulent kinetic energy are generated in the inner boundary layers. Considering the decreasing gradients of the mean velocities and wall normal stresses, the energy production always decreases and totally is zero at Re = 4000 and Ha > 120. This does not match with the increasing/decreasing behavior in case of conducting cylinders, as in [6].

2.3. Flow morphology. Figs. 4 and 5 display that in non-MHD cases the flow at Re = 8000 generates turbulent perturbations of smaller scale than at Re = 4000, due to the larger velocity gradient near the inner cylinder (compare Fig. 4*a* and Fig. 5*a*). At Re = 4000 and a smaller Ha range, we could still find the remaining traces of three pairs of Taylor vortices which are hardly detected at Re = 8000. At the same time, the radial outward jet flows attract small-scale Görtler vortices [11].

Under the influence of the magnetic field, the Taylor vortices keep their shape, and reduce to one pair at Ha = 40 when most of the vortices are still concentrating in the outward jet flow. This particular behavior is better observed at Re = 8000, where the vortices pass through three visible stages: three to two at Ha = 40, two to one at Ha = 60. These evolution processes is also confirmed by the classical linear stability analysis, where the axial magnetic field may stabilize the Taylor-Couette flow with increasing axial wavelength.

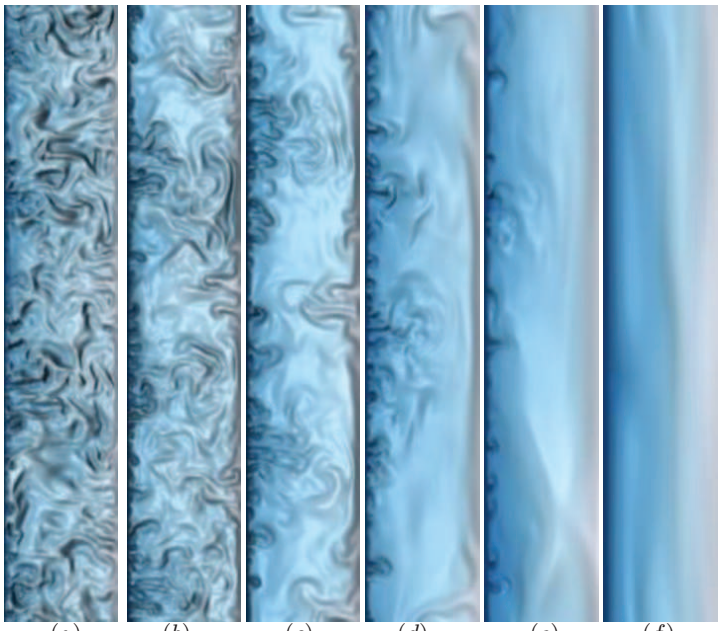

Fig. 5. Instantaneous 2D contours of azimuthal velocity in meridional plane at $\mathrm{Re} = 8000$ with varying Hartmann numbers. (*a*) $\mathrm{Ha} = 0$, $\mathrm{N} = 0$, (*b*) $\mathrm{Ha} = 20$, $\mathrm{N} = 0.05$, (*c*) $\mathrm{Ha} = 40$, $\mathrm{N} = 0.2$, (*d*) $\mathrm{Ha} = 60$, $\mathrm{N} = 0.45$, (*e*) $\mathrm{Ha} = 80$, $\mathrm{N} = 0.8$, and (*f*) $\mathrm{Ha} = 120$, $\mathrm{N} = 1.8$.

The calculation of the turbulent energy production shows that the main part of this energy is injected into the flow near the inner cylinder ($\Delta r_p = r - r_1 \approx 0.05$). One can see that with the growing Ha (or the Stuart number N), the suppression of turbulence occurs everywhere except for the area near the inner cylinder, which keeps serving as a source of turbulence generation (see Figs. 4*b*-*f*, and Figs. 5*b*-*f*).

In the parameter range close to $\mathrm{N} \geq 1$ for both values of Re, the flow patterns are almost similar (compare Figs. 4*c* and 5*d*, Figs. 4*d* and 5*e*, Figs. 4*e* and 5*f*). In Fig. 4*e* and Fig. 5*f*, complete suppression of the turbulence generation and laminarization of the flow are observed there, but with the existence of a weak wave motion. At $\mathrm{N} = 3.6$ in Fig. 4*f*, the wave motion disappears. In the previous case with conducting cylinders [6], the Taylor vortices are destroyed completely even at a smaller magnetic field.

Conclusions. In this study, a direct suppressing effect of the axial magnetic field via dissipating fluctuations has been revealed, which leads to the transformation of the mean flow profiles. Similar to the MHD channel flow [15], the spanwise magnetic field does not affect the Taylor-Couette flow directly, but could change the flow behavior and dynamics by Joule dissipation, introducing anisotropic damping of turbulent fluctuations. It is also revealed that the insulating walls there cause a different flow behavior versus Ha, i.e. instant damping of turbulence as soon as the magnetic field kicks in. Indeed, no enhancement of turbulence in conducting cylinders [5, 6] which is driven by the intensified mean shear and originates from the mean radial current was found. It is concluded that the Stuart number $\mathrm{N} = \mathrm{Ha}^2/\mathrm{Re}$ is the governing parameter for predicting

the effect of the axial magnetic field on turbulence in the Taylor-Couette flow and on its laminarization. Such flows are prone to generate Taylor vortices which are transversal to the axial magnetic field and thus are subject to intensive Joule's dissipation at strong fields. In the presence of the magnetic field, the classical linear sub-layer in the viscous region is maintained and it tends to be extended to a broader area. It is also found that the behavior of MHD turbulence is quite different for two kinds of electric boundary conditions at the cylinder walls. Nevertheless, both of them could be fully suppressed to laminar flow at a very large Hartmann number, even though they have different laminar profiles.

Acknowledgments. The work is supported by the DFG grant KR 4445/2-1, the support from the DFG Research Training Group 1567 is also appreciated. X.Y. Leng acknowledges the supports from the National Natural Science Foundation of China under grant No. 11902224, from the China Postdoctoral Science Foundation under grant No. 2019M651572, and from the Scholarship from the Chinese Scholarship Council.

References

[1] G.I. Taylor. Stability of a viscous liquid contained between two rotating cylinders. *Phil. Trans. R. Soc. A*, vol. 223 (1923), pp. 289–343.

[2] S. Chandrasekhar. *Hydrodynamics and Hydromagnetic Stability* (Dover, New York, 1961).

[3] C.D. Andereck, S.S. Liu, and H.L. Swinney. Flow regimes in a circular Couette system with independently rotating cylinders. *J. Fluid Mech.*, vol. 164 (1986), pp. 155–183.

[4] R.C. Di Prima, and H.L. Swinney. Instabilities and transition in flow between concentric rotating cylinders. In: *Hydrodynamics Instabilities and Transition to Turbulence* (Springer, 1981).

[5] X.Y. Leng, D. Krasnov, Y. Kolesnikov, and B.W. Li. Magnetohydrodynamic Taylor-Couette flow at periodic and Hartmann wall conditions. *Magnetohydrodynamics*, vol. 53 (2017), no. 1, pp. 159–168.

[6] X.Y. Leng, Y. Kolesnikov, D. Krasnov, and B.W. Li. Numerical simulation of turbulent Taylor-Couette flow between conducting cylinders in an axial magnetic field at low magnetic Reynolds number. *Phys. Fluids*, vol. 30 (2018), pp. 015107.

[7] G. Rüdiger, and D. Shalybkov. Stability of axisymmetric Taylor-Couette flow in hydromagnetics. *Phys. Rev. E*, vol. 66 (2002), p. 016307.

[8] H. Ji, and S. Balbus. Angular momentum transport in astrophysics and in the lab. *Phys. Today*, vol. 66 (2013), p. 27.

[9] T. Tagawa, and M. Kaneda. Numerical analyses of a Couette-Taylor flow in the presence of a magnetic field. *J. Phys. Conf. Ser.*, vol. 14 (2005), p. 48.

[10] X.Y. Leng, Y. Yu, and B.W. Li. Numerical study of MHD Taylor vortex flow with low magnetic Reynolds number in finite-length annulus under uniform magnetic field. *Comput. Fluids*, vol. 10 5(2014), pp. 16–27.

[11] S. Dong. Direct numerical simulation of turbulent Taylor-Couette flow. *J. Fluid Mech.*, vol. 587 (2007), pp. 373–393.

[12] P.A. Davidson. *An Introduction to Magnetohydrodynamics* (Cambridge University Press, Cambridge, 2001).

[13] D. Krasnov, O. Zikanov, and T. Boeck. Comparative study of finite difference approaches in simulation of magnetohydrodynamic turbulence at low magnetic Reynolds number. *Comput. Fluids*, vol. 50 (2011), pp. 46–59.

[14] J.C. Adams, P. Swarztrauberg, and R. Sweet. Efficient Fortran subprograms for the solution of separable elliptic partial differential equations. *https://www2.cisl.ucar.edu/resources/legacy/fishpack/*

[15] D. Krasnov, O. Zikanov, J. Schumacher, and T. Boeck. Magnetohydrodynamic turbulence in a channel with spanwise magnetic field. *Phys. Fluids*, vol. 20 (2008), p. 095105.

Received 20.05.2020